

Geophysical Research Letters®

RESEARCH LETTER

10.1029/2024GL109799

T. De Mil and V. Matskovsky contributed equally to this work.

Key Points:

- We present the first X-ray Computed Tomography-derived maximum latewood density-based temperature reconstruction using Bristlecone pine tree cores
- Bristlecone pine maximum latewood density is a reliable proxy for warm-season temperature over a large part of the American Southwest
- Our reconstruction (1625–2005 CE) contains low-frequency variability and can be prolonged over a large part of the Holocene

Supporting Information:

Supporting Information may be found in the online version of this article.

Correspondence to:

T. De Mil,
tom.demil@uliege.be








Citation:

De Mil, T., Matskovsky, V., Salzer, M., Corluy, L., Verschuren, L., Pearson, C., et al. (2024). Bristlecone pine maximum latewood density as a superior proxy for millennium-length temperature reconstructions. *Geophysical Research Letters*, 51, e2024GL109799. <https://doi.org/10.1029/2024GL109799>

Received 13 APR 2024

Accepted 17 JUN 2024

Bristlecone Pine Maximum Latewood Density as a Superior Proxy for Millennium-Length Temperature Reconstructions

T. De Mil¹ , V. Matskovsky^{2,3} , M. Salzer⁴, L. Corluy^{2,3}, L. Verschuren^{2,3,5} , C. Pearson⁴ , L. Van Hoorebeke^{3,6} , V. Trouet^{4,7} , and J. Van den Bulcke^{2,3} 

¹Forest Is Life, TERRA Teaching and Research Centre, Gembloux Agro Bio-Tech, University of Liège, Gembloux, Belgium, ²UGent-Woodlab, Laboratory of Wood Technology, Department of Environment, Ghent University, Ghent, Belgium, ³UGent Centre for X-ray Tomography (UGCT), Ghent, Belgium, ⁴Laboratory of Tree-Ring Research, University of Arizona, Tucson, AZ, USA, ⁵Forest & Nature Lab, Department of Environment, Ghent University, Melle, Belgium, ⁶UGent-Radiation Physics, Department of Physics and Astronomy, Ghent University, Ghent, Belgium, ⁷Belgian Climate Centre, Uccle, Belgium

Abstract Bristlecone pine (*Pinus longaeva*) (PILO) trees exhibit exceptional longevity. Their tree-ring width (TRW) series offer valuable insights into climatic variability. Maximum latewood density (MXD) typically correlates better with temperature variations than TRW, yet PILO MXD records are non-existent due to methodological challenges related to tree-ring structure. Here, we used an X-ray Computed Tomography (X-ray CT) toolchain on 51 PILO cores from the California White Mountains to build a chronology that correlates significantly ($r = 0.66$, $p < 0.01$) with warm-season (March–September) temperature over a large spatial extent. This led to the first X-ray CT-based temperature reconstruction (1625–2005 CE). Good reconstruction skill (RE = 0.51, CE = 0.32) shows that extending MXD records across the full length of the PILO archive could yield a robust warm-season temperature proxy for the American Southwest over millennia. This breakthrough opens avenues for measuring MXD in other challenging conifers, increasing our understanding of past climate further, particularly in lower latitudes.

Plain Language Summary Ancient Bristlecone pine trees can live for several millennia and hold invaluable climate information. Their annual rings were used to develop millennium-length records of the Holocene climate. Maximum latewood density (MXD), which is the highest wood density value in the latewood of a tree ring, has been shown to closely follow summer temperature in different conifer species, but not yet in Bristlecone pine. The gnarly and twisted growth of these ancient trees has presented significant hurdles for MXD analysis. Here we apply an X-ray Computed Tomography toolchain that allows us to 3D scan through the tissue of a tree ring and to map MXD variations. Using this new technique, we were able to reconstruct warm-season temperature for the American Southwest back to 1625 CE. With these findings, we are confident that a full-length reconstruction (back to 2575 BCE) can yield the longest annually resolved temperature reconstruction for this continent.

1. Introduction

Our understanding of temperature variability in the American Southwest over the past centuries to millennia is incomplete (King et al., 2024; Trouet et al., 2013; Wahl et al., 2022). Climatologically speaking, this region is important because of its sensitivity to variability in the El Niño Southern Oscillation system (Cayan et al., 1999) and in the Hadley Circulation (Alfaro-Sánchez et al., 2018). Furthermore, the region is characterized by the past occurrence of multiyear droughts with profound impacts on ecosystems and human systems (Cook et al., 2004; Williams et al., 2020). In contrast to hydroclimate, the temperature history of the American Southwest is less well understood (King et al., 2024). The most highly resolved and precisely dated records of past climate over the Holocene are derived from tree-ring series (Ahmed et al., 2013; Emile-Geay et al., 2017; Esper et al., 2012). For the American Southwest, millennial-length tree-ring chronologies that extend deep into the Holocene are limited to Bristlecone pine (*Pinus longaeva* D.K. Bailey, PILO) records (Salzer et al., 2019). Lower forest border sites such as the iconic Methuselah Walk site (~37.38°N, 118.16°W) (Ferguson, 1968), of which the chronology was recently updated to 8349 BCE (Salzer et al., 2019), provide an accurate estimation of past precipitation variability, but lack a strong temperature signal. Samples from upper treeline sites in the same region have been shown to carry a temperature signal (Kipfmüller & Salzer, 2010; LaMarche & Stockton, 1974; Salzer et al., 2009). Salzer,

© 2024. The Author(s).

This is an open access article under the terms of the [Creative Commons Attribution-NonCommercial-NoDerivs License](https://creativecommons.org/licenses/by/4.0/), which permits use and distribution in any medium, provided the original work is properly cited, the use is non-commercial and no modifications or adaptations are made.

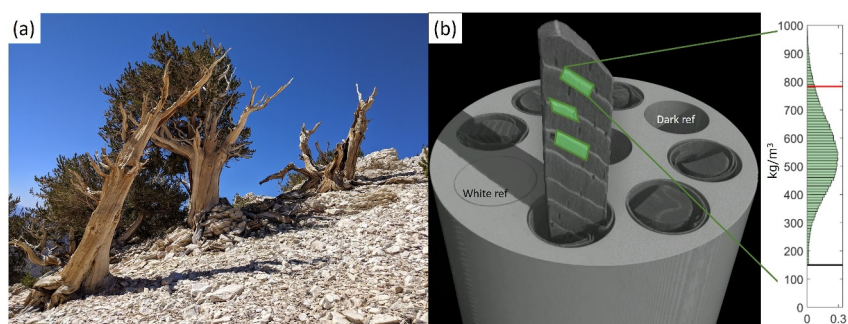


Figure 1. The X-ray Computed Tomography (X-ray CT) toolchain. (a) The iconic Bristlecone pine trees from the California White Mountains, with their gnarly and slow growth that makes their rings hard to measure with traditional X-ray densitometry, (b) an X-ray CT 3D rendered image (created with VGStudio Max from Volume Graphics) of a polymer sample holder with solvent-extracted tree cores in paper straws. Black holes and filled holes are air and reference material respectively to convert gray-value voxels into wood density values. An extracted core from the sample holder is shown where subregions (green) containing the ring boundaries are indicated, and where grain and ring angle are taken into account. The resulting MXD values are calculated by retaining the 95th percentile of the values within this volume (inset). Scanning resolution is 15 μm .

Larson, et al. (2014) developed a tree-ring width (TRW)-based temperature reconstruction (2575 BCE–2006 CE) based on living and dead upper treeline PILO trees. However, the temperature signal in this TRW record is limited to carefully selected trees growing near the very upper treeline (Salzer, Larson, et al., 2014) and is best expressed at (multi-) decadal time scales, rather than annual scales. PILO TRW variability is also influenced by memory effects and by subtle micro-topographical effects (Bruening et al., 2017; Bunn et al., 2011; Tran et al., 2017), which makes an annually resolved temperature reconstruction from the PILO TRW archive challenging. At both high latitudes (Briffa et al., 1988; Esper et al., 2018) and mid latitudes (Büntgen et al., 2010; Klippel et al., 2020; Trouet et al., 2012), maximum latewood density (MXD) has been shown to be a better proxy for summer temperature than TRW. MXD captures the temperature signal at the end of the growing season, when smaller and thicker-walled latewood cells are formed (Rathgeber, 2017). Warmer growing season temperatures generate higher MXD values as the duration of the cell-wall thickening process is extended.

However, the International Tree-Ring Data Bank only has 575 sets of MXD data available globally, compared to over 4,200 sets of TRW data (St. George & Esper, 2019; Zhao et al., 2019). MXD chronologies from low-latitude and semi-arid regions are even more rare. Hence, there is a need to both update and extend MXD chronologies (St. George & Esper, 2019). The main limitation of MXD is the restricted availability of the necessary measurement equipment and its time-consuming nature compared to TRW: fewer than a dozen facilities exist worldwide that conduct conventional X-ray densitometry. Moreover, conventional MXD facilities use measuring equipment that requires the X-ray beams to be parallel to the tracheids (Schweingruber et al., 1978). This has prohibited MXD measurements on PILO samples due to the twisted tracheid angle of the wood, illustrated by its gnarly growth shape (Figure 1a). Nevertheless, PILO records have the potential to drastically extend the current temporal extent of MXD data, which reaches back to 138 BCE (Esper et al., 2012). X-ray Computed Tomography (X-ray CT) has emerged as a valuable tool for deriving TRW and density variables from wood samples with varying grain angles (De Mil et al., 2016; Van den Bulcke et al., 2014). It can be used to correct for grain angle, thus overcoming tedious and destructive laboratory steps and allowing to extract information from deformed tissues (De Mil et al., 2017). X-ray CT has shown its reliability for generating accurate MXD values (Björklund et al., 2019; Bytebier et al., 2022; De Mil et al., 2021).

Here, we apply X-ray CT to PILO samples from the California White Mountains and present the first ever X-ray CT based MXD temperature reconstruction. To achieve this, we (a) measure MXD with X-ray CT, (b) examine the strength of the signal and spatiotemporal stability of the MXD-temperature correlation, and (c) assess skill and compare our reconstruction with other local and regional temperature reconstructions.

2. Materials and Methods

2.1. Scanning and Processing of Tree-Ring Cores

We selected 51 mounted and dated PILO cores from the collection of the Laboratory of Tree-Ring Research (University of Arizona) originating from the California White Mountains site (Figure 1a) (37.57°N 118.21°W–37.51°N 118.17°W). The site contains the following treeline microsites: (a) Sheep Mountain (SHP) (3,395–3,501 m ASL) (24 cores from 23 trees from a field mission in September 2005), (b) South Face (3,445–3,480 m ASL) (14 cores from nine trees sampled in September 2009), and (c) Cottonwood Upper (CWU) (3,470–3,512 m ASL) (13 cores from 10 trees from a field mission in September 2014). Initial pre-selection was based on previous TRW dating, avoiding cores with many missing rings. We unmounted the cores, placed them into paper straws and refluxed in a Soxhlet apparatus for 24 hr in an ethanol/toluene mixture, followed by a 24 hr hot water bath.

We used the X-ray CT toolchain (De Mil & Van den Bulcke, 2023) to non-destructively process the dried and conditioned cores. We scanned the cores at 15 μm approximate volume pixel (voxel) pitch (further referred to as resolution) (70 kV, 20 W, 180 ms, source detector distance 540 mm, source object distance 54 mm, 4,250 projections per full rotation) using a helical scanning procedure (Van den Bulcke et al., 2014) with the CoreTOM scanning system (TESCAN - XRE, Ghent, Belgium). The resulting projections were then reconstructed to 3D volumes using Octopus Reconstruction software (Vlassenbroeck et al., 2007). We then treated the 3D images with the X-CT software (www.dendrochronomics.ugent.be) (De Mil & Van den Bulcke, 2023). We first extracted 3D core volumes from the virtual sample holder (Figure 1b) and then calibrated the volume with the reference material and air hole of the sample holder (De Ridder et al., 2011).

We then indicated tree-ring boundaries using a graphical user interface (De Mil et al., 2016). Small deviations in ring or grain angle can impact the density values (Björklund et al., 2019); therefore, both the radial and transversal planes of the cores were corrected for ring and grain deviations (Van den Bulcke et al., 2014). To avoid resin ducts or wavy ring boundaries, a subvolume was selected for every ring (Figure 1b). To calculate the MXD value for each ring, we selected the 95th percentile of values from all the voxels from this subvolume.

Finally, we checked our TRW series against the crossdated TRW series for the same cores that were previously measured with a Velmex system to 0.001 mm precision (Salzer, Larson, et al., 2014) and exported the MXD data for chronology development.

2.2. Chronology Development and Climate Data

We additionally checked the crossdating of the MXD series using COFECHA software (Holmes, 1983). We used Dplr (Bunn, 2008, 2010) in the R programming environment (R Core Team, 2023) to assess the chronology statistics such as mean interseries correlation (RBAR) and Subsample Signal Strength (SSS) (Wigley et al., 1984), as well as to detrend the series and for chronology building. We tested various detrending options for the MXD data (Figure S1 in Supporting Information S1) and decided to use an age-dependent spline with signal-free implementation (Melvin & Briffa, 2008). Then, we used a bi-weight robust mean to average the obtained dimensionless indices into the final MXD chronology, which was based on 51 dated series with an average length of 259 years and 13,202 measurements in total. We cut the resulting chronology off in 2005, as sample replications drops rapidly thereafter. We extracted monthly mean air temperature and monthly precipitation sums (1895–2005) from the Parameter-elevation Relationships on Independent Slopes Model (PRISM) data set (Daly et al., 2008) using a NetCDF file with 0.25° spatial resolution from KNMI Climate Explorer (Trouet & Van Oldenborgh, 2013). The values were averaged over an area approximately 350 by 350 km (35.1875°–38.1875°N; 119.1458°–115.1458°W) to the east, north and south of the study area, roughly corresponding to the region of the highest correlation between the developed MXD chronology and the gridded mean temperature from PRISM data set. We correlated our MXD chronology (Pearson correlation coefficient) with monthly and seasonal mean climate data, both for the whole period and within a 30-year sliding window. We then selected the seasonal temperature with the strongest correlation with MXD as a reconstruction target. We fit a linear regression model to predict the temperature with the MXD chronology as an independent variable.

To assess the skill of the reconstruction, we performed split calibration-validation tests for 1895–1949 CE and 1950–2005 CE. We calculated correlation in the calibration (r_c) and validation (r_v) periods, coefficient of determination in the calibration period (R_c^2), reduction of error (RE) and coefficient of efficiency (CE) of the

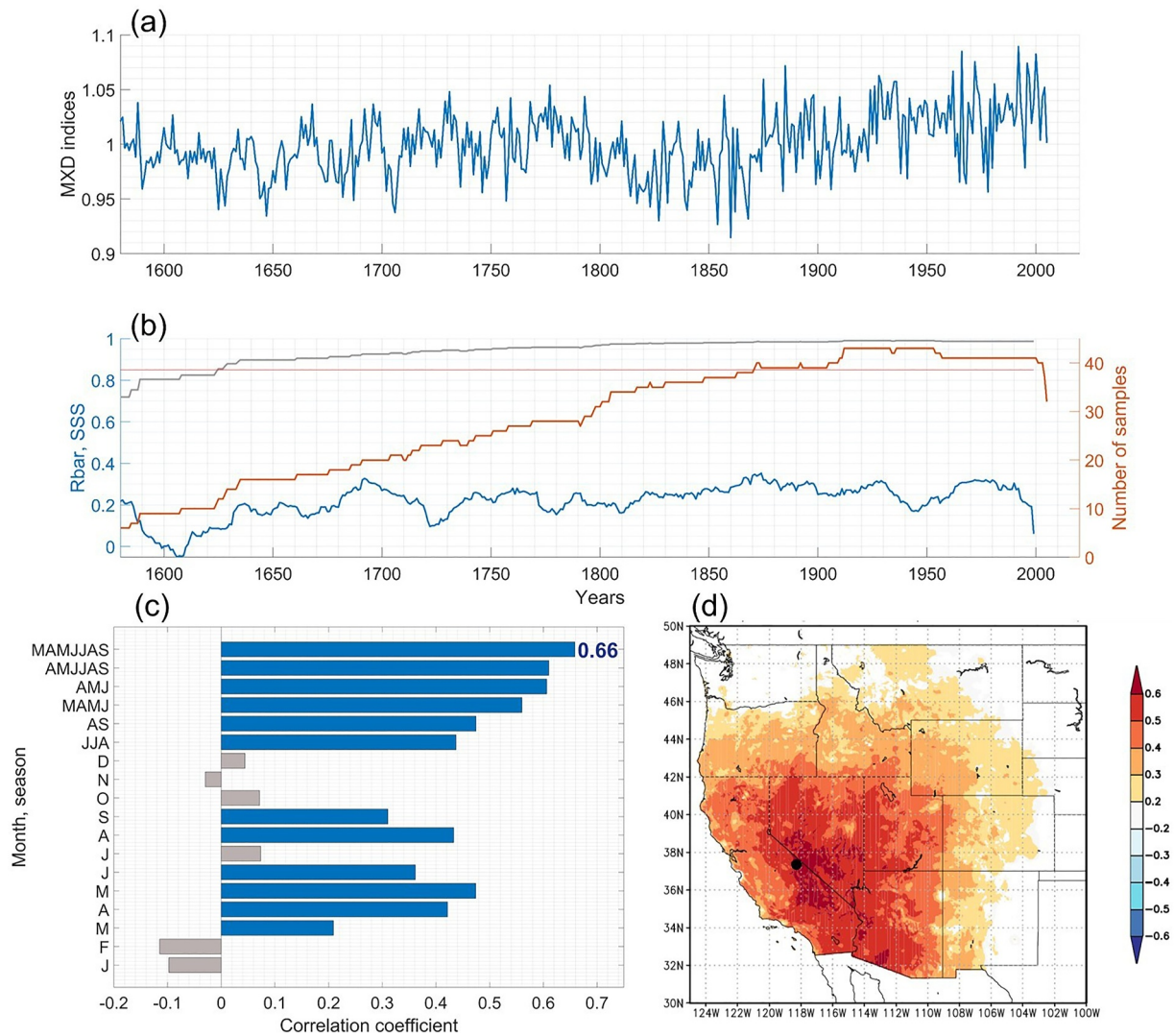


Figure 2. The PILO MXD chronology, its statistics and correlation to climate variables. (a) MXD chronology of PILO. (b) Sample size (orange curve), 30-year (with 15-year lag) running Subsample Signal Strength (SSS) (gray curve) and RBAR (blue curve). Horizontal red line indicates the SSS = 0.85 threshold. (c) Pearson correlation coefficients between the MXD chronology and monthly and seasonal PRISM mean temperature (Daly et al., 2008) for the period 1895–2005 CE. Significant correlations are indicated in blue ($p < 0.05$), and the correlation value for the target season is indicated with a number. (d) Spatial correlation map ($p < 0.10$) between the MXD chronology and mean March–September (MAMJJAS) temperature during 1895–2005 (PRISM data). The map was generated using the KNMI explorer (Trouet & Van Oldenborgh, 2013). Sampling location is marked with a dot.

model (Cook et al., 1994). Then we used the full instrumental period (1895–2005 CE) for the final calibration of the model.

We further generated field correlation maps between our MXD chronology and the PRISM gridded temperature data using the KNMI climate explorer (Trouet & Van Oldenborgh, 2013).

3. Results

3.1. MXD Chronology and Temperature Correlation

The MXD values generated have a mean value of $0.72 \text{ g}\cdot\text{cm}^{-3}$ and a standard deviation of $0.07 \text{ g}\cdot\text{cm}^{-3}$. Mean RBAR and SSS of the resulting MXD chronology (Figure 2a) are 0.255 and 0.948 respectively (Figure 2b). A cut-off of $\text{SSS} > 0.85$ restricted our reconstruction to the earliest date of 1625 CE. For this period, the mean signal-to-noise ratio is 18.12 and the first-order autocorrelation is 0.41. The MXD chronology does not correlate with the TRW chronology ($r = -0.005$, $p = 0.92$). PILO MXD is significantly ($p < 0.05$) positively correlated with

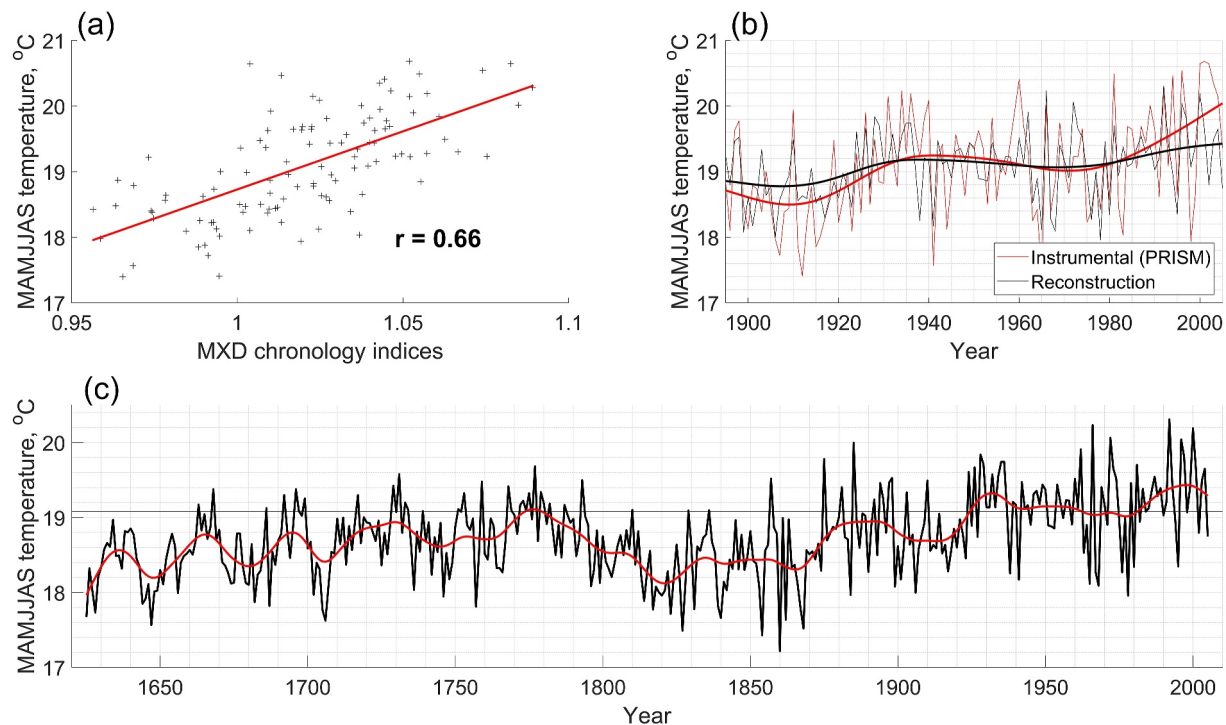


Figure 3. X-ray CT based March–September (MAMJJAS) temperature reconstruction. (a) Scatterplot between mean MAMJJAS temperature and MXD chronology indices. (b) Mean MAMJJAS temperature reconstruction over the instrumental period (1895–2005 CE) (red) and the PRISM temperature data (black). Fifty-year smoothing splines show agreement in the 20th century. (c) Mean MAMJJAS temperature reconstruction for the American Southwest over the 1600–2005 CE period (black), a 25-year smoothing spline is shown in red. The horizontal line reflects the average of the reconstructed values for the 1901–2000 CE period.

monthly mean temperatures from current March to September, with a peak in May and a drop in correlation below the significance level in July (Figure 2c). The strongest correlation coefficients are obtained with the March–September (MAMJJAS) mean temperature ($r = 0.66$, $p < 0.01$). This correlation is temporally stable, which is confirmed by performing a moving window (Figure S2 in Supporting Information S1). Correlation coefficients with precipitation were negative for most months and less significant than for temperature (Figure S3 in Supporting Information S1). TRW records from the same samples yield lower correlations with temperature (Figure S4 in Supporting Information S1). Significant correlations of the PILO MXD record with temperature extend over a large part of the American Southwest (Figure 2d). Correlation coefficients were high ($r > 0.6$, $p < 0.01$) over the Sierra Nevada and the Great Basin and significant ($r > 0.4$, $p < 0.1$) over California, Nevada, Arizona and Utah. Correlation coefficients decrease rapidly to the east of the Rocky Mountains and to the north of the Great Basin, in the states of Oregon, Idaho, Wyoming, Colorado and New Mexico (Figure 2d).

3.2. Reconstruction Potential

A split-period calibration and validation test shows that the MXD chronology carries a robust signal that can be used for reconstruction of mean MAMJJAS surface temperature (Table S1 in Supporting Information S1). The reconstruction explains 43% of the variance in instrumental MAMJJAS temperature (Figures 3a and 3b). Positive RE and CE values on both validation periods (RE = 0.45, CE = 0.27 for 1950–2005, and RE = 0.51, CE = 0.32 for 1895–1949) indicate a good reconstruction potential.

MXD indices and the MAMJJAS mean temperature are generally in a good linear dependence (Figure 3a), which supports the use of a linear regression model for the reconstruction. Good agreement between the MXD chronology and the instrumental temperature data on the inter-annual and decadal time scale also supports the reconstruction potential of the tree-ring data (Figure 3b). At decadal scale (obtained with cubic smoothing splines, 50% variance cut-off at 50-years period) we see that the tree-ring data follow the temperature variations, with an increase in early 20th century until the 1940's, after which a decrease is observed that re-reflects from the 1980's onward. The amplitude of the reconstructed values is lower than that of the instrumental ones by the square root of unexplained variance due to the application of the linear regression method (Esper et al., 2003).

Our American Southwest warm-season temperature reconstruction shows that the most recent two decades (1996–2005) are the warmest since 1625 CE (Figure 3c). Our reconstruction shows cold temperatures during the Little Ice Age that are interrupted by a relatively warm period in the late 18th century (1770–1780 CE). After this short period, there is a rapid cooling in the first half of the 19th century followed by a gradual increase for the rest of the 19th century and throughout the 20th century. The coldest 20-year period observed in our reconstruction is centered around 1823 CE, and the coldest single year is observed in 1860 CE.

4. Discussion and Conclusions

4.1. The Superiority of MXD as a Temperature Proxy

Our warm-season temperature reconstruction for the American Southwest is the first X-ray CT based MXD temperature reconstruction. We found that PILO MXD correlates significantly with a wide 7-month warm-season temperature window (Figure 2c), as was also observed in MXD series of other lower latitude sites, but contrasts with typically narrower seasonal windows at high-latitude sites (Björklund et al., 2017). Tree-ring records are most frequently studied in the extratropical latitudes (40°–90°) (Anchukaitis et al., 2017; Zhao et al., 2019). The prevailing TRW-based paradigm of tree and site selection (Frank et al., 2022; Fritts et al., 1965; St. George, 2014; Wilson et al., 2021) dictates that at lower latitude sites, moisture availability is the dominant limiting factor for tree growth and trees are predominantly sensitive to moisture availability. Lower latitude tree-ring collections are thus predominantly used for hydroclimate reconstructions (Belmecheri et al., 2016). However, sampling of high-elevation sites in these regions increases the strength of the temperature signal (Kipfmüller & Salzer, 2010), which is even more explicitly the case for MXD data (Büntgen et al., 2010; Klippel et al., 2019; Trouet et al., 2012) and confirmed in our study (Figure 2c). MXD RBAR values (Figure 2b) are rather low compared to TRW-based RBAR values from PILO (Salzer, Larson, et al., 2014), which is also observed in other studies, for example, MXD records from the European Alps (Lopez-Saez et al., 2023) or blue intensity records in the Southern Rocky Mountains (Heeter et al., 2020). This is probably due to its lower autocorrelation compared to TRW.

Earlier claims have been made that five-needle conifers, such as PILO, are not suitable for X-ray densitometry due to (a) invariability of the latewood as well as (b) the small rings hindering the standard procedures (F. H. Schweingruber, 1993). Both claims are disputed in our study showing a strong sensitivity of PILO MXD values to warm-season temperature. The strong MXD temperature signal (Figure 3a) ($r = 0.66$) may be further fine-tuned with (a) high-resolution anatomical X-ray CT scanning (Van den Bulcke et al., 2019) or (b) through traditional quantitative wood anatomy (Björklund et al., 2023; Lopez-Saez et al., 2023), however at the expense of significantly lower throughput for both methods.

PILO MXD correlates most strongly with inter-annual temperature variability during those months when cell rehydration and expansion start (April) until cell maturation is completed in September (Ziaco et al., 2016) and thus to the PILO growing season. The correlation gap in July (Figure 2c) is also known as the midsummer decline (Björklund et al., 2017), which has been observed in other species and regions and is more pronounced at lower latitudes. This can be due to July being an intermediate period in the middle of the warm season, with less probability of being affected by lower temperatures, thus not necessarily limiting tree growth (Stine & Huybers, 2017).

4.2. An X-Ray CT Warm-Season Temperature Reconstruction (1625–2005 CE)

Our warm-season temperature reconstruction for the American Southwest (Figure 3c) is one of only a handful of temperature reconstructions for the western part of the USA (Bocinsky & Kohler, 2014; Briffa et al., 1992; King et al., 2024; Salzer, Bunn et al., 2014; Wahl & Smerdon, 2012). In contrast to a previous reconstruction based on TRW from the same PILO sites (Figure 4b), our MXD-based temperature reconstruction preserves inter-annual variability. On a lower frequency scale, our reconstruction matches well with the PILO TRW-based reconstruction (Salzer, Larson, et al., 2014), which signifies the presence of a low-frequency variability in our MXD-based reconstruction.

Like other regional temperature or temperature-related reconstructions (Figure 4), our reconstruction shows a clear recent warming, as well as a distinct warming phase at the end of the 18th century, which co-occurs with a period of increased solar activity (Figure S5 in Supporting Information S1 (SILSO, World Data Center, n.d.)).

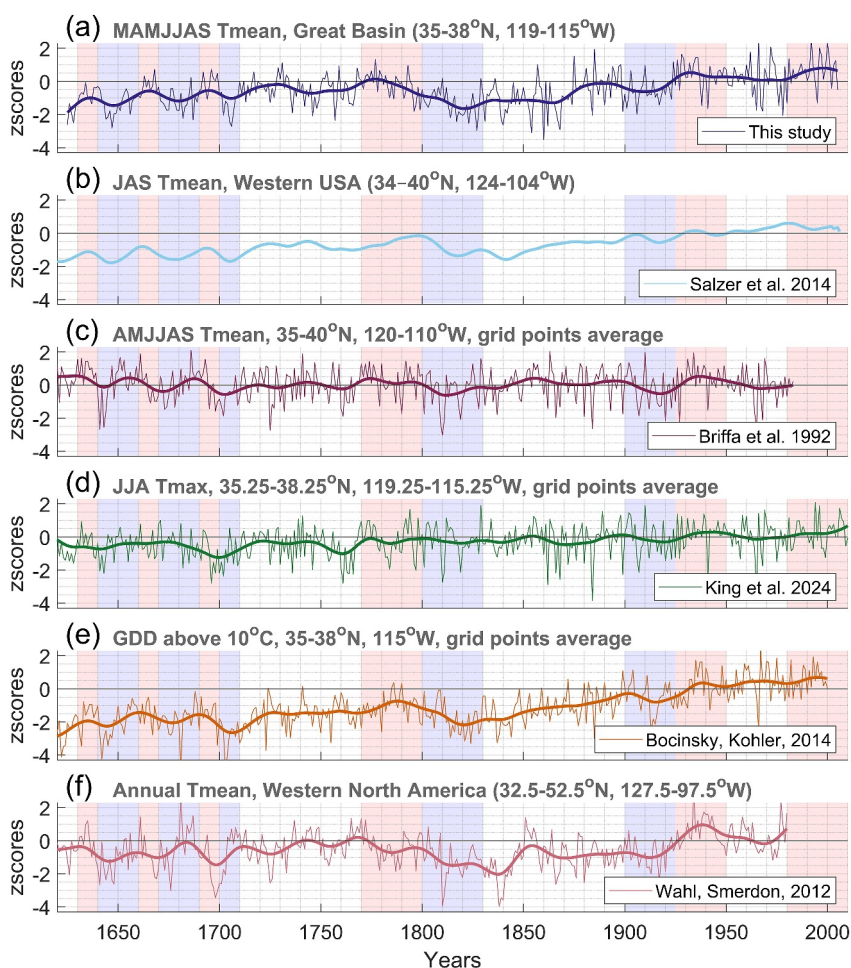


Figure 4. Regional temperature reconstructions from the American West. (a) Our X-ray CT MXD-based MAMJJAS mean temperature reconstruction. (b) Decadal TRW-based JAS temperature reconstruction (Salzer, Bunn et al., 2014) for the Great Basin (USA), based on PILO high-elevation tree-ring collections. (c) AMJJAS air temperature averaged for four nearest gridpoints of the gridded reconstruction (Briffa et al., 1992). (d) JJA maximum temperature reconstruction (King et al., 2024) averaged for the corresponding region. (e) Growing season growing-degree days above 10°C reconstruction (Bocinsky & Kohler, 2014), averaged for three 1° squares of the spatial reconstruction. (f) Annual mean temperature reconstruction for Western North America (Wahl & Smerdon, 2012). Thirty-year splines highlight lower frequency variations. Decadal fluctuations of our reconstruction above or below long-term trends that also correspond to other considered reconstructions are highlighted by pink and blue shading respectively.

This late 18th century warming interrupts a relatively cool Little Ice Age, with its coolest period in the early 19th century, when the Dalton solar minimum coincided with a series of large volcanic eruptions (Raible et al., 2016; Sigl et al., 2015). The warming period at the end of the 18th century, as well as the recent warming, is also visible in other regional and continental temperature reconstructions (Figure 4). Some of the considered reconstructions are quite similar to the reconstruction from this study in terms of both decadal and centennial (Figures 4b–4f) (Wahl & Smerdon, 2012; Bocinsky & Kohler, 2014; Salzer, Larson, et al., 2014; King et al., 2024) variability, while some correlate on higher frequencies (Briffa et al., 1992; King et al., 2024) (Table S2 in Supporting Information S1). Interestingly, the growing-degree days (GDD) reconstruction from Nevada (Figure 4e) (Bocinsky & Kohler, 2014), which is very similar to the reconstruction from this study (Figure 3a, Table S2 in Supporting Information S1), is logically linked by the target climate variable: GDD higher than 10°C should be closely related to the average MAMJJAS temperatures. The reconstruction of Bocinsky and Kohler (2014) has also used tree-ring chronologies as predictors, although the data used is completely independent from our study. Many low-frequency variations of our reconstruction from 1700 onwards closely covary with hemispheric and especially continental-scale temperature variability (Figure S5 in Supporting Information S1).

Given the longevity of PILO and its potential to develop multi-millennia long tree-ring chronologies, the strong temperature signal we found in PILO MXD, as well as the large spatial extent of that signal, provide a strong proof of concept for the successful development of an unprecedented multi-millennial and annual-resolution assessment of past temperature variability in the American Southwest. Furthermore, this new X-ray CT approach for measuring MXD in long-lived and slow-growing trees could be expanded to other regions worldwide that host long-lived, ring-forming species that have a limited temperature signal in their TRW. Examples of such tree species include Rocky Mountains Bristlecone Pine (*Pinus aristata*) in the American Southwest (Salzer & Kipfmüller, 2005; Tintor & Woodhouse, 2021), foxtail pine (*Pinus balfouriana*) (Graumlich, 1993) from the Sierra Nevada, Alerce (*Fitzroya cupressoides*) (Boninsegna & Holmes, 1985) in southern South America, Kauri (*Agathis australis*) in New Zealand (Boswijk et al., 2014), as well as Quillan juniper (*Juniperus przewalskii*) on the Tibetan Plateau (Yang et al., 2014).

Data Availability Statement

The raw MXD measurements, the chronology, as well as the temperature reconstruction, and the files used to generate the Figures are available at Figshare (De Mil et al., 2024).

Acknowledgments

We acknowledge financial support from the Special Research Fund (BOF) for the UGCT Core Facility (BOF-COR.2022.008), from the Research Foundation—Flanders (FWO) for the ACTREAL project (G019521N), the FWO postdoctoral scholarship from TDM (1223020N), and from the IOF for the FaCT project (F2021/IOF-Equip/021). We would like to thank Amy Hudson, Lara Klippel, Isabel Dorado-Linan, Guobao Xu, Diana Zamora-Reyes, Claudia Hartl, Ellie Broadman, Kathy Hirschboeck, Hans Beeckman, Alex Ross, Andy Bunn, Jim Quenelle, William E. Wright, David Frank, Matthew Meko, Malcolm Hughes for the fruitful discussions. Ivan Josipovic, Toon Gheyle, Stijn Willen and Martin Munro for technical and IT support. We are grateful to the craftsmanship of glass blower Tim Gijs.

References

- Ahmed, M., Anchukaitis, K. J., Asrat, A., Borgaonkar, H. P., Braidia, M., Buckley, B. M., et al. (2013). Continental-scale temperature variability during the past two millennia. *Nature Geoscience*, 6(5), 339–346. <https://doi.org/10.1038/ngeo1797>
- Alfaro-Sánchez, R., Nguyen, H., Klesse, S., Hudson, A., Belmecheri, S., Köse, N., et al. (2018). Climatic and volcanic forcing of tropical belt northern boundary over the past 800 years. *Nature Geoscience*, 11(12), 933–938. <https://doi.org/10.1038/s41561-018-0242-1>
- Anchukaitis, K. J., Wilson, R., Briffa, K. R., Büntgen, U., Cook, E. R., D'Arrigo, R., et al. (2017). Last millennium Northern Hemisphere summer temperatures from tree rings: Part II, spatially resolved reconstructions. *Quaternary Science Reviews*, 163, 1–22. <https://doi.org/10.1016/j.quascirev.2017.02.020>
- Belmecheri, S., Babst, F., Wahl, E. R., Stahle, D. W., & Trouet, V. (2016). Multi-century evaluation of Sierra Nevada snowpack. *Nature Climate Change*, 6(1), 2–3. <https://doi.org/10.1038/nclimate2809>
- Björklund, J., Seftigen, K., Schweingruber, F., Fonti, P., Von Arx, G., Bryukhanova, M. V., et al. (2017). Cell size and wall dimensions drive distinct variability of earlywood and latewood density in Northern Hemisphere conifers. *New Phytologist*, 216(3), 728–740. <https://doi.org/10.1111/nph.14639>
- Björklund, J., Seftigen, K., Stoffel, M., Fonti, M. V., Kottlow, S., Frank, D. C., et al. (2023). Fennoscandian tree-ring anatomy shows a warmer modern than medieval climate. *Nature*, 620(7972), 97–103. <https://doi.org/10.1038/s41586-023-06176-4>
- Björklund, J., von Arx, G., Nievergelt, D., Wilson, R., Van den Bulcke, J., Günther, B., et al. (2019). Scientific merits and analytical challenges of tree-ring densitometry. *Reviews of Geophysics*, 57(4), 1224–1264. <https://doi.org/10.1029/2019RG000642>
- Bocinsky, R. K., & Kohler, T. A. (2014). A 2,000-year reconstruction of the rain-fed maize agricultural niche in the US Southwest. *Nature Communications*, 5(1), 5618. <https://doi.org/10.1038/ncomms6618>
- Boninsegna, J. A., & Holmes, R. L. (1985). *Fitzroya cupressoides* yields 1534-year long South American chronology. *Tree-Ring Bulletin*, 45, 37–42.
- Boswijk, G., Fowler, A. M., Palmer, J. G., Fenwick, P., Hogg, A., Lorrey, A., & Wunder, J. (2014). The late Holocene kauri chronology: Assessing the potential of a 4500-year record for palaeoclimate reconstruction. *Quaternary Science Reviews*, 90, 128–142. <https://doi.org/10.1016/j.quascirev.2014.02.022>
- Briffa, K. R., Jones, P. D., & Schweingruber, F. H. (1988). Summer temperature patterns over Europe: A reconstruction from 1750 A.D. based on maximum latewood density indices of conifers. *Quaternary Research*, 30(1), 36–52. [https://doi.org/10.1016/0033-5894\(88\)90086-5](https://doi.org/10.1016/0033-5894(88)90086-5)
- Briffa, K. R., Jones, P. D., & Schweingruber, F. H. (1992). Tree-ring density reconstructions of summer temperature patterns across western North America since 1600. *Journal of Climate*, 5(7), 735–754. [https://doi.org/10.1175/1520-0442\(1992\)005<0735:trdros>2.0.co;2](https://doi.org/10.1175/1520-0442(1992)005<0735:trdros>2.0.co;2)
- Bruening, J. M., Tran, T. J., Bunn, A. G., Weiss, S. B., & Salzer, M. W. (2017). Fine-scale modeling of Bristlecone pine treeline position in the Great Basin, USA. *Environmental Research Letters*, 12(1), 014008. <https://doi.org/10.1088/1748-9326/aa5432>
- Bunn, A. G. (2008). A dendrochronology program library in R (dplR). *Dendrochronologia*, 26(2), 115–124. <https://doi.org/10.1016/j.dendro.2008.01.002>
- Bunn, A. G. (2010). Statistical and visual crossdating in R using the dplR library. *Dendrochronologia*, 28(4), 251–258. <https://doi.org/10.1016/j.dendro.2009.12.001>
- Bunn, A. G., Hughes, M. K., & Salzer, M. W. (2011). Topographically modified tree-ring chronologies as a potential means to improve paleoclimate inference: A letter. *Climatic Change*, 105(3–4), 627–634. <https://doi.org/10.1007/s10584-010-0005-5>
- Büntgen, U., Frank, D., Trouet, V., & Esper, J. (2010). Diverse climate sensitivity of Mediterranean tree-ring width and density. *Trees - Structure and Function*, 24(2), 261–273. <https://doi.org/10.1007/s00468-009-0396-y>
- Bytbeier, J., De Mil, T., Vanhellemont, M., Verheyen, K., Haneca, K., & Van den Bulcke, J. (2022). Linking wood density records of common beech (*Fagus sylvatica* L.) with temperature and precipitation variability from a temperate lowland site. *Dendrochronologia*, 76, 126018. <https://doi.org/10.1016/j.dendro.2022.126018>
- Cayan, D. R., Redmond, K. T., & Riddle, L. G. (1999). ENSO and hydrologic extremes in the western United States. *Journal of Climate*, 12(9), 2881–2893. [https://doi.org/10.1175/1520-0442\(1999\)012<2881:EAHEIT>2.0.CO;2](https://doi.org/10.1175/1520-0442(1999)012<2881:EAHEIT>2.0.CO;2)
- Cook, E. R., Briffa, K. R., & Jones, P. D. (1994). Spatial regression methods in dendroclimatology: A review and comparison of two techniques. *International Journal of Climatology*, 14(4), 379–402. <https://doi.org/10.1002/joc.3370140404>
- Cook, E. R., Woodhouse, C. A., Eakin, C. M., Meko, D. H., & Stahle, D. W. (2004). Long-term aridity changes in the western United States. *Science*, 306(5698), 1015–1018. <https://doi.org/10.1126/science.1102586>

- Daly, C., Halbleib, M., Smith, J. I., Gibson, W. P., Doggett, M. K., Taylor, G. H., et al. (2008). Physiographically sensitive mapping of climatological temperature and precipitation across the conterminous United States. *International Journal of Climatology*, 28(15), 2031–2064. <https://doi.org/10.1002/joc.1688>
- De Mil, T., Angoboy Ilondea, B., Maginet, S., Duvillier, J., Van Acker, J., Beeckman, H., & Van den Bulcke, J. (2017). Cambial activity in the understory of the Mayombe forest, DR Congo. *Trees - Structure and Function*, 31(1), 49–61. <https://doi.org/10.1007/s00468-016-1454-x>
- De Mil, T., Matskovsky, V., Salzer, M. W., Corluy, L., Verschuren, L., Pearson, C., et al. (2024). Bristlecone pine maximum latewood density from the California White Mountains and March-to-September temperature reconstruction for American Southwest [Dataset]. *Figshare*. <https://doi.org/10.6084/m9.figshare.25562499>
- De Mil, T., Meko, M., Belmecheri, S., February, E., Therrell, M., Van den Bulcke, J., & Trouet, V. (2021). A lonely dot on the map: Exploring the climate signal in tree-ring density and stable isotopes of Clanwilliam cedar, South Africa. *Dendrochronologia*, 69, 125879. <https://doi.org/10.1016/j.dendro.2021.125879>
- De Mil, T., & Van den Bulcke, J. (2023). Tree core analysis with X-ray Computed Tomography. *Journal of Visualized Experiments: JoVE*, 199, e65208. <https://doi.org/10.3791/65208>
- De Mil, T., Vannoppen, A., Beeckman, H., Van Acker, J., & Van Den Bulcke, J. (2016). A field-to-desktop toolchain for X-ray CT densitometry enables tree ring analysis. *Annals of Botany*, 117(7), 1187–1196. <https://doi.org/10.1093/aob/mcw063>
- De Ridder, M., Van Den Bulcke, J., Vansteenkiste, D., Van Loo, D., Dierick, M., Masschaele, B., et al. (2011). High-resolution proxies for wood density variations in *Terminalia superba*. *Annals of Botany*, 107(2), 293–302. <https://doi.org/10.1093/aob/mcq224>
- Emile-Geay, J., McKay, N. P., Kaufman, D. S., von Gunten, L., Wang, J., Anchukaitis, K. J., et al. (2017). A global multiproxy database for temperature reconstructions of the Common Era. *Scientific Data*, 4(1), 170088. <https://doi.org/10.1038/sdata.2017.88>
- Esper, J., Cook, E. R., Krusic, P. J., Peters, K., Schweingruber, F. H., Citation Esper, J., et al. (2003). Tests of the RCS method for preserving low-frequency variability in long tree-ring chronologies item type article. Retrieved from <http://hdl.handle.net/10150/262573>
- Esper, J., Frank, D. C., Timonen, M., Zorita, E., Wilson, R. J. S., Luterbacher, J., et al. (2012). Orbital forcing of tree-ring data. *Nature Climate Change*, 2(12), 862–866. <https://doi.org/10.1038/nclimate1589>
- Esper, J., George, S. S., Anchukaitis, K., D'Arrigo, R., Ljungqvist, F. C., Luterbacher, J., et al. (2018). *Large-scale, millennial-length temperature reconstructions from tree-rings*. Dendrochronologia. Elsevier GmbH. <https://doi.org/10.1016/j.dendro.2018.06.001>
- Ferguson, C. W. (1968). Bristlecone pine: Science and esthetics. *Science*, 159(3817), 839–846. <https://doi.org/10.1126/science.159.3817.839>
- Frank, D., Fang, K., & Fonti, P. (2022). Dendrochronology: Fundamentals and Innovations. In R. T. W. Siegwolf, J. R. Brooks, J. Roden, & M. Saurer (Eds.), *Stable isotopes in tree rings: Inferring physiological, climatic and environmental responses* (pp. 21–59). Springer International Publishing. https://doi.org/10.1007/978-3-030-92698-4_2
- Fritts, H., Smith, D., Cardis, J., & Budelsky, C. (1965). Tree-ring Characteristics along a vegetation gradient in Northern Arizona. *Ecology*, 46(4), 394–401. <https://doi.org/10.2307/1934872>
- Graumlich, L. J. (1993). A 1000-year record of temperature and precipitation in the Sierra Nevada. *Quaternary Research*, 39(2), 249–255. <https://doi.org/10.1006/qres.1993.1029>
- Heeter, K. J., Harley, G. L., Maxwell, J. T., McGee, J. H., & Matheus, T. J. (2020). Late summer temperature variability for the Southern Rocky Mountains (USA) since 1735 CE: Applying blue light intensity to low-latitude *Picea engelmannii* Parry ex Engelm. *Climatic Change*, 162(2), 965–988. <https://doi.org/10.1007/s10584-020-02772-9>
- Holmes, R. L. (1983). Computer-assisted quality control in tree-ring dating and measurement. *Tree-Ring Bulletin*, 43, 69–78.
- King, K. E., Cook, E. R., Anchukaitis, K. J., Cook, B. I., Smerdon, J. E., Seager, R., et al. (2024). Increasing prevalence of hot drought across western North America since the 16th century. *Science Advances*, 4289(4), 1–10. <https://doi.org/10.1126/sciadv.adj4289>
- Kipfmüller, K. F., & Salzer, M. W. (2010). Linear trend and climate response of five-needle pines in the western United States related to treeline proximity. *Canadian Journal of Forest Research*, 40(1), 134–142. <https://doi.org/10.1139/X09-187>
- Klippel, L., Büntgen, U., Konter, O., Kyncl, T., & Esper, J. (2020). Climate sensitivity of high- and low-elevation *Larix decidua* MXD chronologies from the Tatra Mountains. *Dendrochronologia*, 60, 125674. <https://doi.org/10.1016/j.dendro.2020.125674>
- Klippel, L., Krusic, P. J., Konter, O., St. George, S., Trouet, V., & Esper, J. (2019). A 1200+ year reconstruction of temperature extremes for the northeastern Mediterranean region. *International Journal of Climatology*, 39(4), 2336–2350. <https://doi.org/10.1002/joc.5955>
- LaMarche, V. C., & Stockton, C. W. (1974). Chronologies from temperature-sensitive bristlecone pines at upper treeline in western United States. *Tree-Ring Bulletin*, 34, 21–45.
- Lopez-Saez, J., Corona, C., von Arx, G., Fonti, P., Slamova, L., & Stoffel, M. (2023). Tree-ring anatomy of *Pinus cembra* trees opens new avenues for climate reconstructions in the European Alps. *Science of the Total Environment*, 855, 158605. <https://doi.org/10.1016/j.scitotenv.2022.158605>
- Melvin, T. M., & Briffa, K. R. (2008). A “signal-free” approach to dendroclimatic standardisation. *Dendrochronologia*, 26(2), 71–86. <https://doi.org/10.1016/j.dendro.2007.12.001>
- Raible, C. C., Brönnimann, S., Auchmann, R., Brohan, P., Frölicher, T. L., Graf, H. F., et al. (2016). Tambora 1815 as a test case for high impact volcanic eruptions: Earth system effects. *Wiley Interdisciplinary Reviews: Climate Change*, 7(4), 569–589. <https://doi.org/10.1002/wcc.407>
- Rathgeber, C. B. K. (2017). Conifer tree-ring density interannual variability - Anatomical, physiological and environmental determinants. *New Phytologist*, 216(3), 621–625. <https://doi.org/10.1111/NPH.14763>
- R Core Team. (2023). R: A language and environment for statistical computing. [Computer software manual]. Vienna, Austria. Retrieved from <https://www.R-project.org/>
- Salzer, M. W., Bunn, A. G., Graham, N. E., & Hughes, M. K. (2014a). Five millennia of paleotemperature from tree-rings in the Great Basin, USA. *Climate Dynamics*, 42(5–6), 1517–1526. <https://doi.org/10.1007/s00382-013-1911-9>
- Salzer, M. W., Hughes, M. K., Bunn, A. G., & Kipfmüller, K. F. (2009). Recent unprecedented tree-ring growth in bristlecone pine at the highest elevations and possible causes. *Proceedings of the National Academy of Sciences of the United States of America*, 106(48), 20348–20353. <https://doi.org/10.1073/pnas.0903029106>
- Salzer, M. W., & Kipfmüller, K. F. (2005). Reconstructed temperature and precipitation on a millennial timescale from tree-rings in the southern Colorado Plateau, U.S.A. *Climatic Change*, 70(3), 465–487. <https://doi.org/10.1007/s10584-005-5922-3>
- Salzer, M. W., Larson, E. R., Bunn, A. G., & Hughes, M. K. (2014). Changing climate response in near-treeline bristlecone pine with elevation and aspect. *Environmental Research Letters*, 9(11), 114007. <https://doi.org/10.1088/1748-9326/9/11/114007>
- Salzer, M. W., Pearson, C. L., & Baisan, C. H. (2019). Dating the methuselah walk bristlecone pine floating chronologies. *Tree-Ring Research*, 75(1), 61–66. <https://doi.org/10.3959/1536-1098-75.1.61>
- Schweingruber, F., Fritts, H., Braker, O., Drew, L., & Schar, E. (1978). The Xray technique as applied to dendroclimatology. *Tree-Ring Bulletin*, 38, 61–91.

- Schweingruber, F. H. (1993). Tree Species in North America. In *Trees and Wood in Dendrochronology: Morphological, Anatomical, and Tree-Ring Analytical Characteristics of Trees Frequently Used in Dendrochronology* (pp. 208–342). Springer Berlin Heidelberg. https://doi.org/10.1007/978-3-642-77157-6_4
- Sigl, M., Winstrup, M., McConnell, J. R., Welten, K. C., Plunkett, G., Ludlow, F., et al. (2015). Timing and climate forcing of volcanic eruptions for the past 2,500 years. *Nature*, 523(7562), 543–549. <https://doi.org/10.1038/nature14565>
- SILSO, World Data Center. (n.d.). SILSO, World Data Center - Sunspot Number and Long-term Solar Observations, Royal Observatory of Belgium, on-line Sunspot Number catalogue, 1700–2005. Retrieved from <http://www.sidc.be/SILSO/>
- St. George, S. (2014). An overview of tree-ring width records across the Northern Hemisphere. *Quaternary Science Reviews*, 95, 132–150. <https://doi.org/10.1016/j.quascirev.2014.04.029>
- St. George, S., & Esper, J. (2019). Concord and discord among Northern Hemisphere paleotemperature reconstructions from tree rings. *Quaternary Science Reviews*, 203, 278–281. <https://doi.org/10.1016/j.quascirev.2018.11.013>
- Stine, A. R., & Huybers, P. (2017). Implications of Liebig's law of the minimum for tree-ring reconstructions of climate. *Environmental Research Letters*, 12(11), 114018. <https://doi.org/10.1088/1748-9326/aa8cd6>
- Tintor, W. L., & Woodhouse, C. A. (2021). The variable climate response of Rocky Mountain bristlecone pine (*Pinus aristata* Engelm.). *Dendrochronologia*, 68, 125846. <https://doi.org/10.1016/j.dendro.2021.125846>
- Tran, T. J., Bruening, J. M., Bunn, A. G., Salzer, M. W., & Weiss, S. B. (2017). Cluster analysis and topoclimate modeling to examine bristlecone pine tree-ring growth signals in the Great Basin, USA. *Environmental Research Letters*, 12(1), 014007. <https://doi.org/10.1088/1748-9326/aa5388>
- Trouet, V., Diaz, H. F., Wahl, E. R., Viau, A. E., Graham, R., Graham, N., & Cook, E. R. (2013). A 1500-year reconstruction of annual mean temperature for temperate North America on decadal-to-multidecadal time scales. *Environmental Research Letters*, 8(2), 024008. <https://doi.org/10.1088/1748-9326/8/2/024008>
- Trouet, V., Panayotov, M. P., Ivanova, A., & Frank, D. (2012). A pan-European summer teleconnection mode recorded by a new temperature reconstruction from the northeastern Mediterranean (ad 1768–2008). *The Holocene*, 22(8), 887–898. <https://doi.org/10.1177/0959683611434225>
- Trouet, V., & Van Oldenborgh, G. J. (2013). KNMI climate explorer: A web-based research tool for high-resolution paleoclimatology. *Tree-Ring Research*, 69(1), 3–13. <https://doi.org/10.3959/1536-1098-69.1.3>
- Van Den Bulcke, J., Boone, M. A., Dhaene, J., Van Loo, D., Van Hooebeke, L., Boone, M. N., et al. (2019). Advanced X-ray CT scanning can boost tree ring research for earth system sciences. *Annals of Botany*, 124(5), 837–847. <https://doi.org/10.1093/aob/mcz126>
- Van den Bulcke, J., Wernersson, E. L. G., Dierick, M., Van Loo, D., Masschaele, B., Brabant, L., et al. (2014). 3D tree-ring analysis using helical X-ray tomography. *Dendrochronologia*, 32(1), 39–46. <https://doi.org/10.1016/j.dendro.2013.07.001>
- Vlassenbroeck, J., Dierick, M., Masschaele, B., Cnudde, V., Van Hooebeke, L., & Jacobs, P. (2007). Software tools for quantification of X-ray microtomography at the UGCT. *Nuclear Instruments and Methods in Physics Research, Section A: Accelerators, Spectrometers, Detectors and Associated Equipment*, 580(1 SPEC. ISS.), 442–445. <https://doi.org/10.1016/j.nima.2007.05.073>
- Wahl, E. R., & Smerdon, J. E. (2012). Comparative performance of paleoclimate field and index reconstructions derived from climate proxies and noise-only predictors. *Geophysical Research Letters*, 39(6), 1–5. <https://doi.org/10.1029/2012GL051086>
- Wahl, E. R., Zorita, E., Diaz, H. F., & Hoell, A. (2022). Southwestern United States drought of the 21st century presages drier conditions into the future. *Communications Earth and Environment*, 3(1), 1–14. <https://doi.org/10.1038/s43247-022-00532-4>
- Wigley, T. M. L., Briffa, K. R., & Jones, P. D. (1984). On the average value of correlated time series with applications in dendroclimatology and hydrometeorology. *Journal of Climate & Applied Meteorology*, 23(2), 201–213. [https://doi.org/10.1175/1520-0450\(1984\)023<0201:OTAVOC>2.0.CO;2](https://doi.org/10.1175/1520-0450(1984)023<0201:OTAVOC>2.0.CO;2)
- Williams, A. P., Cook, E. R., Smerdon, J. E., Cook, B. I., Abatzoglou, J. T., Bolles, K., et al. (2020). Erratum for the Report "Large contribution from anthropogenic warming to an emerging North American megadrought" by A. Park Williams, E. R. Cook, J. E. Smerdon, B. I. Cook, J. T. Abatzoglou, K. Bolles, S. H. Baek, A. M. Badger, B. Livneh. *Science*, 370(6516), 314–318. <https://doi.org/10.1126/SCIENCE.ABF3676>
- Wilson, R., Allen, K., Baker, P., Boswijk, G., Buckley, B., Cook, E., et al. (2021). Evaluating the dendroclimatological potential of blue intensity on multiple conifer species from Tasmania and New Zealand. *Biogeosciences*, 18(24), 6393–6421. <https://doi.org/10.5194/bg-18-6393-2021>
- Yang, B., Qin, C., Wang, J., He, M., Melvin, T. M., Osborn, T. J., & Briffa, K. R. (2014). A 3,500-year tree-ring record of annual precipitation on the northeastern Tibetan Plateau. *Proceedings of the National Academy of Sciences of the United States of America*, 111(8), 2903–2908. <https://doi.org/10.1073/pnas.1319238111>
- Zhao, S., Pederson, N., D'Orangeville, L., HilleRisLambers, J., Boose, E., Penone, C., et al. (2019). The International Tree-Ring Data Bank (ITRDB) revisited: Data availability and global ecological representativity. *Journal of Biogeography*, 46(2), 355–368. <https://doi.org/10.1111/jbi.13488>
- Ziaco, E., Biondi, F., Rossi, S., & Deslauriers, A. (2016). Environmental drivers of cambial phenology in Great Basin bristlecone pine. *Tree Physiology*, 36(7), 818–831. <https://doi.org/10.1093/treephys/tpw006>